scientific reports

OPEN

Revisiting the magnetic structure of Holmium at high pressure by using neutron diffraction

M. Pardo-Sainz[1,2], F. Cova[1], J. A. Rodríguez-Velamazán[3], I. Puente-Orench[1], Y. Kousaka[4], M. Mito[5] & J. Campo[1✉]

Low-temperature neutron diffraction experiments at $P = 8$ GPa have been conducted to investigate the magnetic structures of metallic Holmium at high pressures by employing a long d-spacing high-flux diffractometer and a Paris-Edinburgh press cell inside a cryostat. We find that at $P = 8$ GPa and $T = 5$ K, no nuclear symmetry change is observed, keeping therefore the hexagonal closed packed (*hcp*) symmetry at high pressure. Our neutron diffraction data confirm that the ferromagnetic state does not exist. The magnetic structure corresponding to the helimagnetic order, which survives down to 5 K, is fully described by the magnetic superspace group formalism. These results are consistent with those previously published using magnetization experiments.

Magnetism of itinerant electrons[1] have played an important role in condensed matter physics to explain the properties of ferromagnetic metals. In particular, in the 3d transition metals based on Fe, Co, and Ni, the mechanism responsible for their ferromagnetism can be understood within the Stoner model[2].

On the other hand, the ferromagnetism in the 4f-electron lanthanide metals, such as Gd, Tb, Dy, Ho, Er, and Tm, is explained by the Ruderman–Kasuya–Kittle–Yosida (RKKY) interaction between localized moments of the 4f-electrons mediated by the conduction electrons[3–5]. The spatially damped oscillation of the spin polarization of the conduction electrons is responsible of the competition between the ferromagnetic (FM) and antiferromagnetic (AFM) interactions, which often results in an incommensurate helimagnetic structure (HM).

The RKKY interaction constant (J_{RKKY}) is highly sensible to subtle lattice contractions that happen at low temperatures. This could destabilize the HM state giving place to a FM ground state. Hereafter, the magnetic transition temperatures between the FM and HM states and between the HM and the paramagnetic (PM) states are denoted as T_C and T_N, respectively.

The structure of all 4f-lanthanide FM metals is hexagonal closed packed, *hcp*, with stacking unit ABA at ambient pressure (AP), and exhibit the structural transformations in the sequence *hcp* (ABA) → Sm-type (ABABCB-CACA) → double-*hcp* (*dhcp*) (ABACA) → *fcc* (ABCA) → trigonal under increasing pressure[6,7].

The evoution of the magnetic properties with the structural transformations in 4f-lanthanide metals has been studied theoretically[8] and reported experimentally by magnetic characterization[9–13], electrical resistivity[14–20], neutron diffraction[14,16,21–25], X-ray diffraction[26], and Mössbauer spectroscopy[27]. In particular, neutron diffraction experiments have been successfully employed to study the magnetic phases of Ho metal at high pressures and variable temperatures, as we briefly summarize in the next paragraph.

The first neutron scattering experiment in this metal was performed at AP by Koehler et al.[28]. They reported that Ho magnetic moments form a basal plane helix below $T_N = 133$ K, and a conical configuration, with a net magnetic moment parallel to the c-axis, below $T_C = 20$ K, in agreement with later neutron experiments[29,30]. In year 1968, Umebayashi et al.[21] studied Tb and Ho at pressures below 1 GPa and temperatures above 80 K, where the pressure dependences of T_N and the helical turn angle were measured. It was found that the HM ordering is shifted to lower temperatures when the pressure is increased. In 1988, Achiwa et al.[31] studied the Ho metal up to 2.1 GPa in the temperature range 10 K to T_N. The helical pitch angle evolution with temperature was found in agreement with Ref.[21] for $P = 0.6$ GPa, while for higher pressures the values of the angle increased showing a lock-in value below 20 K.

[1]Instituto de Nanociencia y Materiales de Aragón (CSIC – Universidad de Zaragoza) and Depto. de Física de la Materia Condensada, C/Pedro Cerbuna 12, 50009 Zaragoza, Spain. [2]Graduate School of Science, Osaka Metropolitan University, 1-1 Gakuencho, Sakai, Osaka 599-8531, Japan. [3]Institut Laue Langevin, 71 avenue des Martyrs CS 20156, 38042 Grenoble Cedex 9, France. [4]Department of Physics and Electronics, Osaka Metropolitan University, 1-1 Gakuencho, Sakai, Osaka 599-8531, Japan. [5]Graduate School of Engineering, Kyushu Institute of Technology, Kitakyushu 804-8550, Japan. ✉email: javier.campo@csic.es

Recently, the new available extreme conditions neutron diffractometers have facilitated the study of the high pressure region of Holmium. In 2012, Thomas et al.[14] performed neutron diffraction experiments at maximum pressures of 6.6 GPa at 89, 110 and 300 K. They established the incommensurate nature of the HM phase and determined the decrease of T_N from approximately 122 K at AP at a rate of -4.9 K/GPa up to a pressure of 9 GPa, above which the PM to HM transition vanishes, in agreement with Ref.[21,31]. In 2020, Perreault et al.[25] performed neutron diffraction experiments at maximum pressures of 20 GPa and temperatures above of 10 K. They observed two magnetic transitions below 10 GPa: one to an incommensurate HM phase and another to a conical FM phase. For pressures above 10 GPa in the Sm-type phase, and above 19 GPa in the *dhcp* phase, the appearance of a magnetic peak at 3 Å and the increase of the intensity of some nuclear peaks were assigned to the presence of a FM ordering below 30 K.

The P dependence of T_N and T_C, evaluated with magnetic susceptibility[11] (black-empty symbols), a.c and d.c magnetization[12,13] (blue and red filled symbols), and neutron diffraction[25] (green-empty symbols) is showed for Ho in the magnetic phase diagram in Fig. 1.

In our recent a.c. magnetization measurements, using a superconducting quantum interference device (SQUID) magnetometer at zero applied magnetic field (H_{dc} = 0 T), the signal of the FM anomaly was reduced below any detectable level at a pressure between 5.7 and 8.8 GPa[13]. The anomaly at 5.7 GPa suggested a first order phase transition that remained in the range 0.5–11.6 GPa after remeasuring the sample by decreasing the pressure from 11.2 GPa (the results in the sequence after 11.2 GPa are not visible in Fig. 1 but details can be found in ref.[13]). Thus, residual strain influenced the suppression of the FM order.

On the other hand, in d.c. magnetization measurements at H_{dc} = 0.5 T, which is one-third of the critical field to the saturated state, the FM anomaly was still observed at 7.3 GPa, and a broad hump appeared at 9.2 GPa[12]. It suggested that the FM order becomes unstable above 7.3 GPa and a short range order composed of small grains is developed at 9.2 GPa. In different magnetization measurements, using a SQUID vibrating-coil-magnetometer method, the development of a ferromagnetic magnetization was observed at 8.2 GPa, which disappeared at 12 GPa[13]. All these facts together stressed that the P region between 8 and 12 GPa is a critical region to understand the FM ordering.

Thus, different series of magnetic measurements showed that; (i) the HM transition was observed at pressures up to 12 GPa, while the FM transition seems to be unstable at approximately 8 GPa, and (ii) the ferromagnetic short range ordering could survive until approximately 11 GPa[12,13].

However, previous neutron diffraction experiments, covering a d spacing between 1.0 and 3.5 Å, reported that the FM ordering survives until at least 20 GPa[25]. Therefore, it seems that a controversy exists between the
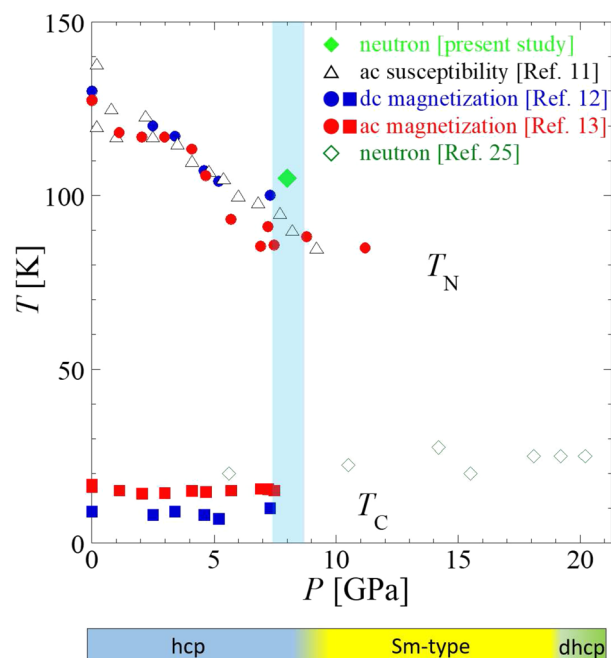

Figure 1. P dependence of T_N and T_C for Ho[11–13]. The green point at $P = 8$ GPa and $T_N = 105$ K has been determined in this study. Blue and red symbols correspond to the data obtained from our previous magnetic characterization studies using an SQUID magnetometer, while the black empty triangles and green empty diamonds correspond to the previous a.c. susceptibility and neutron diffraction experiments, respectively. The size of the error bars, in temperature and pressure, is smaller than the size of the symbols employed. The color bar at the bottom part of the figure indicates the different phase transformations happening as the pressure increases at room temperature according to ref.[32]. The present study focuses on the light-blue shaded region.

last neutron diffraction experiments by Perreault et al.[25] and the macroscopic magnetic characterization of Ho at high pressures[12,13].

With the aim to elucidate this controversy, in the present study, by performing neutron powder diffraction experiments, but covering a wide d-spacing region ($1.4 \leq d \leq 50$ Å), we determined the magnetic structure at 8 GPa, in the temperature range $5 \leq T \leq 300$ K. The magnetic superspace group (MSSG) formalism[33–35] has been employed to classify the symmetry of the magnetic structure.

High pressure neutron diffraction experiments

Polycrystalline sample of metallic natural Ho with high purity (99.999%) was purchased from Sigma-Aldrich. Especial care was taken to manipulate the sample minimizing the exposure time to air.

Neutron powder diffraction experiments were carried out on the high-flux 2-axis neutron diffractometer D1B of the Institut Laue-Langevin (ILL) in Grenoble, France. This instrument has a MWGC 1D-detector spanning an angular range of $128°$ with a definition of $0.1°$. A Radial Oscillating Collimator (ROC) was installed in order to eliminate the spurious signals produced by the sample environment.

Two data acquisitions were taken at AP and room temperature (RT) for a Ho powder sample inside a 6 mm diameter vanadium can, with neutron wavelengths of $\lambda = 1.28$ Å and 2.52 Å which allowed to explore d-spacings, respectively, of 0.7–15.0 Å and 1.4–50 Å.

The data collection at 8 GPa were performed with $\lambda = 2.52$ Å which correspond to the maximum flux configuration of the D1B instrument. For these acquisitions, the powder was placed in a null-scattering TiZr gasket using a deuterated 4:1 ethanol-methanol mix as pressure transmitter medium, (the same that the one employed before by Perreault et al. at 20 GPa[25]), which is the typical in all the neutron diffraction experiments. Then, it was introduced inside a VX5/180 Paris-Edinburgh (PE) pressure cell[36,37] equipped with SINE-type sintered diamond anvils[38]. A pressure of 0.12 GPa was applied to the PE cell, for which the sample corresponded to 8 GPa, after calibration with a Pb flake placed with the sample. Then the PE cell was cooled using liquid nitrogen and helium from RT to 5 K. At this temperature, a 4.5 hours isotherm acquisition was performed. Then the sample was warmed back to RT in 10 hours and diffractograms were collected every 15 minutes.

It is well known that the 4:1 ethanol-methanol mixture is not the *ideal* transmitting media at low temperatures but it is a good approach to the hydrostatic behavior at room temperature for pressures below 10 GPa[39]. Furthermore, the fact that we do not detect any remarkable change, with decreasing the temperature, with the sample inside the PE cell, neither in the background of the diffractograms, nor in the width of the Bragg lines (see Fig. 3), suggests that the quality of the pressure at 5 K is good enough in our experimental conditions.

Different crystallographic tools were employed for the determination of the crystal and magnetic structures, which include the FullProf Suite[40], the ISODISTORT Suite[41,42], and utilities within the Bilbao Crystallographic Server[43–46] for the symmetry analysis and visualization.

Results and analysis

P = 0 GPa. Figure 2 shows the diffraction patterns collected with wavelengths $\lambda = 1.28$ Å (top) and 2.52 Å (bottom). The peaks observed in the diffraction patterns at AP and RT can be indexed by the paramagnetic $P6_3/mmc.1'$ MSSG (No. 194.264). This crystal structure corresponds with a hcp structure where the Ho atom is located in the Wyckoff position (WP) $2c$, with coordinates (1/3 2/3 1/4). The cell parameters obtained from a multi-pattern refinement of both diffractograms are: $a = b = 3.5690(2)$Å, $c = 5.6020(4)$ Å, $\alpha = \beta = 90°$, $\gamma = 120°$; with $R_{Bragg} = 15.1$ and 11.2, for $\lambda = 1.28$ Å and 2.52 Å, respectively.

P = 8 GPa. Insert of Fig. 3 shows the diffraction pattern collected with $\lambda = 2.52$ Å at $P = 8$ GPa and $T = 5$ K. The first remarkable fact is the presence of a new high-intensity peak observed at $d \sim 21$ Å that was not present in the diffractograms taken at RT. The low part of the Fig. 3 shows a zoom of the small d-spacing region for the diffractograms collected at $T = 5$ K (middle part) and RT (bottom part) with the sample inside the PE cell in the cryostat. With this complex sample environment, once the sample is inside the gasket in the PE cell, the intensity is greatly suppressed, since for high pressure experiments the quantity of sample irradiated by the neutron beam is much smaller. Additionally, a huge increase of the background and a broad feature around 3.7 Å are observed even with the ROC in front of the detector, mainly due to the large incoherent scattering of hydrogen from the pressure transmitting fluid[47].

The diffractogram observed at RT inside the PE cell, after warming from 5 K, reveals the presence of two distinct sets of reflections. The first set corresponds to the Pb flake, where the reflections are indexed by the cubic space group $Fm\bar{3}m$ (No. 225), with Pb atoms occupying the WP $4a$[48] (see purple diamonds label in Fig. 3). By analysing the position of the reflection (2 0 0), located at $d = 2.367(1)$ Å, we can determine the cell parameter to be $a = 4.734(2)$ Å. This information allows us to derive a volume per atom of $V = 26.52(3)$ Å^3/atom, which, when considering the equations of state presented in[49,50], yields a pressure of 8.0(1) GPa. The other set of reflections corresponds to the Ho sample and is indexed by the same hcp structure ($P6_3/mmc.1'$) with shorter cell parameters ($a = b = 3.4030(7)$ Å, $c = 5.345(2)$ Å, and $R_{Bragg} = 6.07$) than the one observed at AP. Therefore, no structural transition to the Sm-type phase has been observed as the pressure was increased from AP to 8 GPa.

However, at 8 GPa and 5 K, several new magnetic satellites appear, marked with red and orange asterisks in Fig. 3, including the one clearly observed at $d \sim 21$ Å. These satellites are indexed with an incommensurate propagation vector $\vec{k}_{HM} = (0\,0\,\delta)$ with $\delta = \pm 0.2536(1)$, in units of c^*, in agreement with Ref.[25]. The plus or minus sign in the propagation vector indicates a clock-wise or anti clock-wise propagation. The nuclear peaks, marked with black and grey asterisks in Fig. 3, remain unchanged respect to the ones at RT, suggesting that no FM order is present, even at the lowest temperature. The analysis of this new magnetic state will be elucidated in the next subsection.
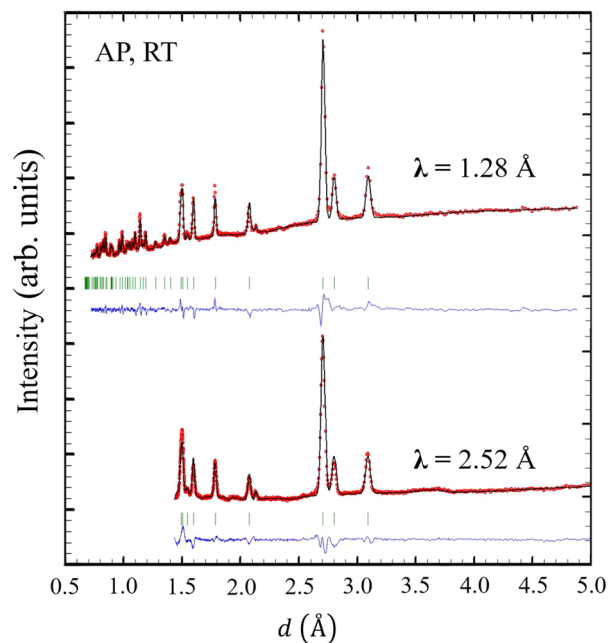
Figure 2. Diffraction patterns collected with $\lambda = 1.28$ Å (up) and 2.52 Å (down) at RT and AP. In red are shown the observed points and in black continuous line the calculated pattern with the parameters described in the main text. The blue continuous line and the green ticks indicate, the difference between the observed and calculated profile, and the nuclear peaks generated by the space group, respectively.

Regarding the reflections due to the Pb flake, at 5 K the reflection $(2\,0\,0)$ can still be observed at $d = 2.367(1)$ Å, which ensures that the pressure was kept constant (within a 0.1 GPa range) during the warming process.

Symmetry analysis. We use the symmetry analysis to reduce the number of possible magnetic ground states in Ho-*hcp* compatible with the observed propagation vector $\vec{k}_{HM}$. We can decompose the magnetic representation for the Ho atom, located at WP 2*c*, as a direct sum of Irreducible Representations (*irreps*) of the parent group $P6_3/mmc.1'$ for the Δ point, $(0\,0\,\delta)$, of the Brillouin zone (BZ) (we adopted the international notation for the *irreps* labels and MSSG established in[41–43]), as follows:

$$m\Gamma_{2c} = 1m\Delta_2(1) \oplus 1m\Delta_3(1) \oplus 1m\Delta_5(2) \oplus 1m\Delta_6(2).$$

The basis vectors of each *irrep* are given in Table 1. The magnetic structure described by both, the 1d-*irreps* mΔ_2 and mΔ_3 consists of a sinusoidal modulation along the *c*-axis. Meanwhile, the 2d-*irreps*, mΔ_5 and mΔ_6, describe helices in which the magnetic moments are contained in ferromagnetic *ab* planes, and propagate along the *c*-axis. However, both models differ greatly when considering the phase-shift between the Ho atoms in the unit cell. While in the case of mΔ_6 the phase-shift is the same as the pitch angle of the helix: $\phi = 180 \times k_{HM} = \pm45.65(2)°$, in m$\Delta_5$ the phase-shift is given by: $\phi = 180 \times (k_{HM} + 1) = \pm225.65(2)°$. Therefore, the magnetic structure given by mΔ_6 can be considered as a single helix, while for mΔ_5 the system is composed of two independent helices, one for each atom in the unit cell. The magnetic structure at 5 K, labelled with mΔ_6, and the ϕ angle are depicted in Fig. 4.

After a systematic trial and error procedure, it was observed that mΔ_2, mΔ_3 and mΔ_5 do not fit the data, since they assign zero intensity for the main magnetic peak indexed as $(0\,0\,0) \pm \vec{k}_{HM}$ at $d \sim 21$ Å. However, the magnetic satellite reflections (red and orange asterisks in Fig. 3) can be correctly fitted by the 2d-*irrep* mΔ_6.

The combination between the parent group $P6_3/mmc.1'$ and the magnetic modulations for Ho atoms given by the *irrep* mΔ_6 give as a result the $P6_322.1'(0\,0\,\gamma)h00s$ MSSG. Within the MSSG formalism, the magnetic structure is described by a basic structure, related to the nuclear paramagnetic cell, in addition to a series of magnetic modulation functions that describe the variation from the basic structure of the magnetic moments. In our case, with just one propagation vector $\vec{k}_{HM}$ and no net magnetic moment (i.e. no existence of a propagation vector $\vec{k}_{FM} = (0\,0\,0)$), the magnetic structure is described by:

$$\vec{M}_{lj} = \vec{M}_{j,s} \sin(2\pi x_4) + \vec{M}_{j,c} \cos(2\pi x_4),$$

where the internal coordinate x_4 is given by the product of the propagation vector and the position $\vec{r}_{lj}$ of the atom j in the l-th unit cell ($x_4 = \vec{k}_{HM} \cdot \vec{r}_{lj}$).

The explicit amplitudes of the cosine ($\vec{M}_{j,c}$) and sine ($\vec{M}_{j,s}$) components of the magnetic moment for the $P6_322.1'(0\,0\,\gamma)h00s$ MSSG are given in Table 2. In this MSSG, the Ho atom remains in the WP 2*c* position and
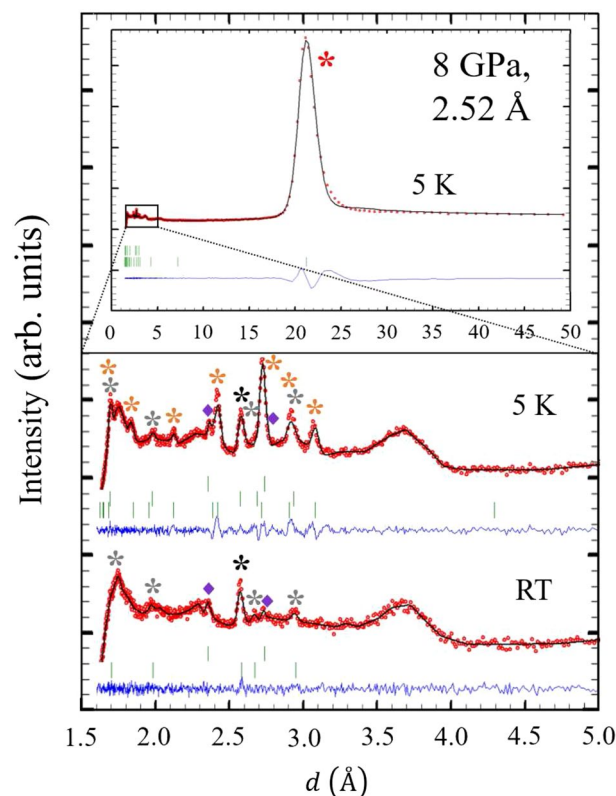
Figure 3. The insert shows the 5 K diffractogram in the full d-spacing scale accessible with the neutron wavelength $\lambda = 2.52$ Å at 8 GPa. A large magnetic signal appears at ~ 21 Å . A zoom of the small d-spacing region of the diffractograms collected with $\lambda = 2.52$ Å is displayed in the middle part (5 K) and bottom part (RT) of the figure. In red are shown the observed points and in back continuous line the calculated pattern with the parameters described in the main text. The blue continuous line and the green ticks indicate the difference between the observed and calculated profile and the nuclear and satellite peaks generated by the magnetic superspace group, respectively. Red and orange asterisks label the satellite peaks visible only in the HM phase. Black and grey asterisks label the nuclear peaks visible at both temperatures. Purple diamonds label the peaks due to the Pb flake. The broad feature around 3.7 Å is due to the pressure transmitting fluid and treated as a background contribution.

irrep	BV	Ho1 (1/3 2/3 1/4)	Ho2 (2/3 1/3 3/4)
mΔ_2	ψ_1^2	$(0\,0\,1)$	$(0\,0\,1)e^{-i\pi\delta}$
mΔ_3	ψ_1^3	$(0\,0\,1)$	$(0\,0\,\bar{1})e^{-i\pi\delta}$
mΔ_5	ψ_1^5	$\left(1-\frac{1}{\sqrt{3}}\,i,\,-\frac{2}{\sqrt{3}}\,i,\,0\right)$	$\left(1-\frac{1}{\sqrt{3}}\,i,\,-\frac{2}{\sqrt{3}}\,i,\,0\right)e^{-i\pi(\delta+1)}$
	ψ_2^5	$\left(-\frac{2}{\sqrt{3}}\,i,\,1-\frac{1}{\sqrt{3}}\,i,\,0\right)$	$\left(-\frac{2}{\sqrt{3}}\,i,\,1-\frac{1}{\sqrt{3}}\,i,\,0\right)e^{-i\pi(\delta+1)}$
mΔ_6	ψ_1^6	$\left(1-\frac{1}{\sqrt{3}}\,i,\,-\frac{2}{\sqrt{3}}\,i,\,0\right)$	$\left(1-\frac{1}{\sqrt{3}}\,i,\,-\frac{2}{\sqrt{3}}\,i,\,0\right)e^{-i\pi\delta}$
	ψ_2^6	$\left(-\frac{2}{\sqrt{3}}\,i,\,1-\frac{1}{\sqrt{3}}\,i,\,0\right)$	$\left(-\frac{2}{\sqrt{3}}\,i,\,1-\frac{1}{\sqrt{3}}\,i,\,0\right)e^{-i\pi\delta}$

Table 1. Basis vectors (BV) of each *irrep* present in the magnetic representation of the Ho 2c site for the space group $P6_3/mmc.1'$ with $\vec{k}_{HM} = (0\,0\,\delta)$. The basis vectors components are expressed in terms of the crystallographic axis a, b and c.

the symmetry constraints imposed allow only for 1 free parameter to describe the magnetic structure, which is the modulus of the magnetic moment (M).

Temperature dependence. Figure 5 shows a 2D plot of the thermo-diffractograms obtained at 8 GPa as the system was heated from 5 K to RT. From them, the onset of the helical magnetic ordering is estimated to occur around $T_N = 105(2)$ K, with the appearance of a peak at $d \sim 21$ Å ($2\theta \sim 7°$), which is in agreement with previous studies[11–13,25].
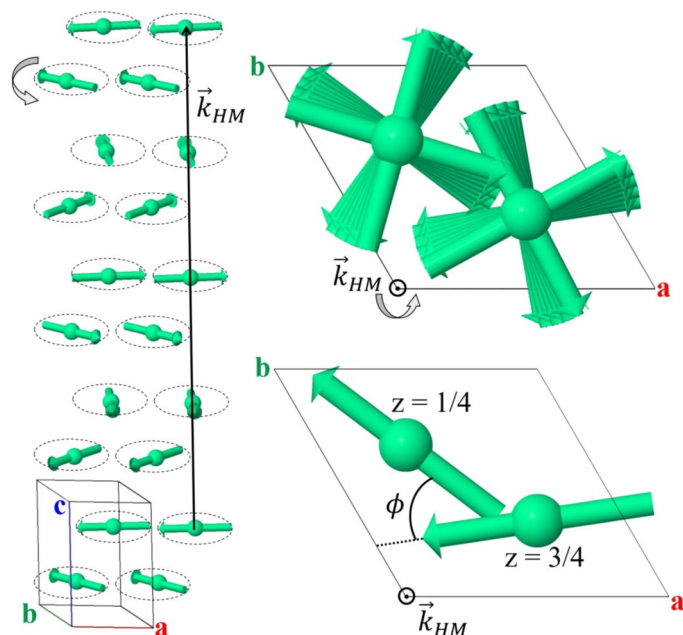
Figure 4. Magnetic structure obtained from the refinement of the data with the model given by the $P6_322.1'(0\,0\,\gamma)h00s$ MSSG. Five nuclear unit cells along c axis are shown. The right bottom side shows the pitch angle ϕ formed by the magnetic moments in adjacent ferromagnetic ab planes along c. The right upper side shows a projection of the magnetic moments onto the ab planes.

Phase	PM	HM
T (K)	300	5
MSSG	$P6_3/mmc.1'$	$P6_322.1'(0\,0\,\gamma)h00s$
#	194.264	182.1.24.2.m180.2
$\vec{k}$		$(0\,0\,\delta)$
δ		0.2536(1)
$\phi\,(°)$		45.65(2)
irrep		$m\Delta_6$
a (Å)	3.4030(7)	3.3976(6)
c (Å)	5.345(2)	5.390(1)
c/a	1.5707(7)	1.5864(4)
$\vec{M}_c$		$M(0\,1\,0)$
$\vec{M}_s$		$M\left(\frac{-2}{\sqrt{3}}\,\frac{-1}{\sqrt{3}}\,0\right)$
$M(\mu_B)$		6.94(1)
R_{Bragg}	6.07	6.64
$R_{\text{Bragg}}(\text{Mag.})$		1.59

Table 2. Structural and magnetic parameters for Ho metallic at 8 GPa and $T =$300 and 5 K obtained from the analysis of the patterns collected at D1B. The cosine ($\vec{M}_{j,c}$) and sine ($\vec{M}_{j,s}$) components of the magnetic moment are expressed in terms of the crystallographic axis a, b and c.

The temperature dependence of the intensity for the (1 0 1) nuclear reflection (in black) and the satellite $(0\,0\,0) \pm \vec{k}_{\text{HM}}$ (in red) is shown in Fig. 6b. The evolution of these two lines allows to quantitatively distinguish between the magnetic phases that can be present, as the nuclear and satellite peaks chosen should be the most sensible if a FM ($\vec{k}_{\text{FM}} = (0\,0\,0)$) or HM order ($\vec{k}_{\text{HM}}$), respectively, should be present. No change is observed neither in the (1 0 1) nuclear reflection, nor other nuclear lines, as the temperature decreases. This fact supports the hypothesis of absence of any FM ordering, or if present, put an upper limit of $0.2\mu_B$ to such contribution.

Regarding the evolution with temperature of the satellite $(0\,0\,0) \pm \vec{k}_{\text{HM}}$, its intensity was fitted to the power law $I \propto \epsilon^{2\beta}$, where $\epsilon = T_N - T$ is the reduced temperature (see Fig. 7). The obtained value for the critical exponent is $\beta = 0.40(1)$, which is in good agreement with the value predicted by Bak and Mukamel[51], and reported by
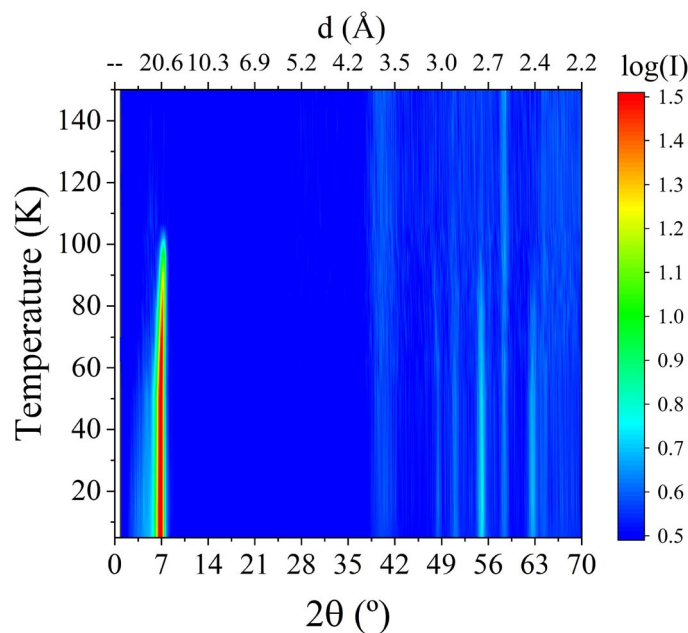
Figure 5. 2D plot of the thermo-diffractograms measured at 8 GPa with $\lambda = 2.52$ Å as the system was heated from 5 K to RT. The appearance of the peak at $d \sim 21$ Å($2\theta \sim 7°$) is clearly visible at $T = 105(2)$ K.

previous studies for pure helimagnetic phases at AP and 130 K conditions[52–55]. It constitutes another indication of the absence of any FM component.

Using the magnetic model labelled by the $P6_322.1'(0\,0\,\gamma)h00s$ MSSG to fit the diffraction patterns collected at each temperature, the dependence of the pitch angle, ϕ, and modulus, M, of the Ho magnetic moment versus temperature was obtained (see Fig. 6c).

As the temperature decreases below $T_N \sim 105(2)$ K, the magnetic moment increases until it saturates at $6.94(1)\mu_B$, a value in good agreement with the saturation magnetization obtained at AP and $T = 5$ K[12]. Meanwhile, the ϕ angle decreases following two linear dependences from $48.6(1)°$ at 105 K to $45.65(2)°$ at 5K, with a change of slope around $T \sim 40$ K. This evolution is also coherent with previous neutron diffraction experiments[25], and can be understood if we consider the strong dependence of the helix period with the axial ratio c/a of the hexagonal phase[8]. Such dependence can also explain the change observed around 40 K, since the ratio c/a is stabilized below that temperature (see Fig. 6a).

Discussion

In our last study using SQUID magnetization measurements it was reported that the HM order survives up to $P = 12$ GPa, while the disappearance of the FM order, or, at least, a remarkable suppression of ferromagnetic net magnetic moments, was observed above 8 GPa[13]. As the intensity of the FM anomaly could not be detected just above the critical pressure for the phase boundary between the *hcp* and Sm-type phases, it was suggested that the disappearance of the FM order is related to the structural phase transition.

However, the present neutron diffraction experiments, focused on the magnetic structure at $P = 8$ GPa, confirm that the *hcp* structure remains stable until at least 8 GPa. Additionally, an incommensurate HM order is observed below $T_N = 105(2)$ K, which persists down to the lowest temperature measured ($T = 5$ K), while no evidence of FM ordering was observed within the entire temperature range. Therefore, the present results help to clarify that the FM order becomes unstable and disappear just before the structural phase transition. Furthermore, the magnetic structure observed at 8 GPa is consistent with previous magnetic measurements, taking into account the pressure distribution with the order of ±0.5 GPa during the high-pressure experiment.

In the neutron diffraction study by Perreault et al., the FM order was reported to survive in both the Sm-type phase at 14.2 GPa and the *dhcp* phase at 20.2 GPa[25]. This FM transition was marked by the appearance of a magnetic peak at $d = 3$ Å accompanied by an increase in the intensity of all nuclear peaks. However, in those experiments only a small region of d-spacing (1.0–3.5 Å) was covered, which made it difficult to elucidate the additional existence of HM order at those pressures, since the expected most intense magnetic signal should appear at larger d-spacing (see Fig. 3). Therefore, it would be interesting to confirm those results by performing neutron experiments at such pressures in a long d-spacing diffractometer.

Conclusion

We conducted neutron diffraction experiments to investigate the magnetic structures of Ho at $P = 8$ GPa. Our findings indicate that the nuclear symmetry remains unchanged, preserving the hexagonal close-packed (*hcp*) symmetry at $P = 8$ GPa. The helimagnetic order persists down to 5 K, and the analysis of its magnetic structure,

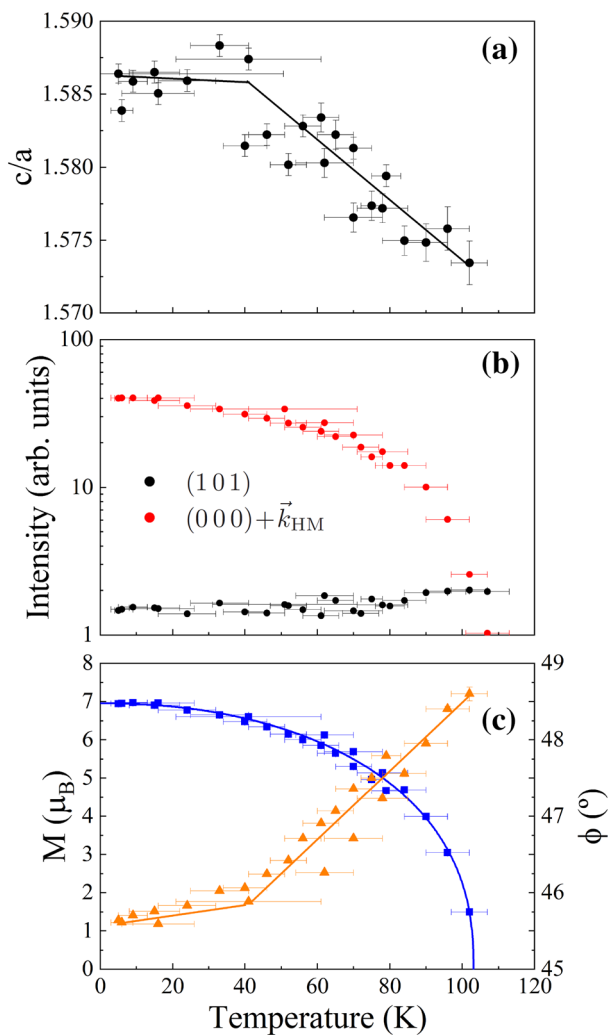**Figure 6.** (**a**) Temperature dependence of the ratio c/a. (**b**) Logarithmic scale plot of the intensity evolution with temperature for the nuclear peak $(1\,0\,1)$ (black) and the satellite reflection $(0\,0\,0) \pm \vec{k}_{HM}$ (red). These peaks are marked with black and red asterisks in the diffractograms of Fig. 3. (**c**) Temperature dependence of the modulus $M(\mu_B)$ (blue squares) and ϕ angle values (orange triangles). The lines are a guide to the eyes. A change in the linear behaviour of ϕ is observed at around 40 K.
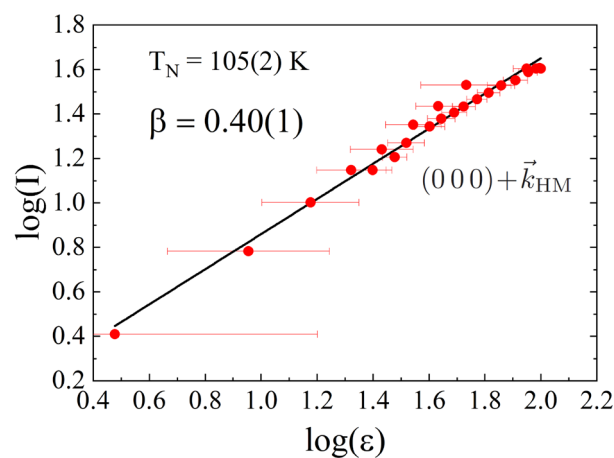
Figure 7. Logarithmic plot of the intensity of the satellite reflection $(0\,0\,0) \pm \vec{k}_{HM}$ as a function of the reduced temperature. The value of the transition temperature T_N was estimated from Fig. 5.

using the magnetic superspace group formalism, allows to determine the critical exponent $\beta = 0.40(1)$, in agreement with previous theoretical model for pure helices. Meanwhile no FM contribution is observed at any temperature. These results are consistent with previously published findings from magnetization experiments.

References

1. Chikazumi, S. *Physics of Ferromagnets* (Oxford University Press, 1997).
2. Stoner, E. C. Collective electron ferromagnetism II. Energy and specific heat. *Proc. R. Soc. Lond. A* **169**, 339–371 (1939).
3. Ruderman, M. & Kittel, C. Indirect exchange coupling of nuclear magnetic moments by conduction electrons. *Phys. Rev.* **96**, 99. https://doi.org/10.1103/PhysRev.96.99 (1954).
4. Kasuya, T. A theory of metallic ferro-and antiferromagnetism on Zener's model. *Prog. Theor. Phys.* **16**, 45–57. https://doi.org/10.1143/PTP.16.45 (1956).
5. Yosida, K. Magnetic properties of Cu–Mn alloys. *Phys. Rev.* **106**, 893. https://doi.org/10.1103/PhysRev.106.893 (1957).
6. Akella, J., Smith, G. S. & Jephcoat, A. P. High-pressure phase transformation studies in gadolinium to 106 GPa. *J. Phys. Chem. Solids* **49**, 573–576. https://doi.org/10.1016/0022-3697(88)90069-8 (1988).
7. Grosshans, W. & Holzapfel, W. Atomic volumes of rare-earth metals under pressures to 40 GPa and above. *Phys. Rev. B* **45**, 5171. https://doi.org/10.1103/PhysRevB.45.5171 (1992).
8. Hughes, I. D. *et al.* Lanthanide contraction and magnetism in the heavy rare earth elements. *Nature* **446**, 650–653. https://doi.org/10.1038/nature05668 (2007).
9. McWhan, D. & Stevens, A. Effect of pressure on the magnetic properties and crystal structure of Gd, Tb, Dy, and Ho. *Phys. Rev.* **139**, A682. https://doi.org/10.1103/PhysRev.139.A682 (1965).
10. Iwamoto, T., Mito, M., Hitaka, M., Kawae, T. & Takeda, K. Magnetic measurement of rare earth ferromagnet gadolinium under high pressure. *Physica B* **329–333**, 667–668. https://doi.org/10.1016/S0921-4526(02)02516-4 (2003).
11. Jackson, D. D., Malba, V., Weir, S. T., Baker, P. A. & Vohra, Y. K. High-pressure magnetic susceptibility experiments on the heavy lanthanides Gd, Tb, Dy, Ho, Er, and Tm. *Phys. Rev. B* **71**, 184416. https://doi.org/10.1103/PhysRevB.71.184416 (2005).
12. Mito, M. *et al.* Volume shrinkage dependence of ferromagnetic moment in the lanthanide ferromagnets gadolinium, terbium, dysprosium, and holmium. *J. Phys. Chem. Solids* **70**, 1290–1296. https://doi.org/10.1016/j.jpcs.2009.07.013 (2009).
13. Mito, M. *et al.* Relationship of magnetic ordering and crystal structure in lanthanide ferromagnets Gd, Tb, Dy, and Ho at high pressures. *Phys. Rev. B* **103**, 24444. https://doi.org/10.1103/PhysRevB.103.024444 (2021).
14. Thomas, S. A. *et al.* Neutron diffraction and electrical transport studies on the incommensurate magnetic phase transition in holmium at high pressures. *J. Phys. Condens. Matter* **24**, 216003. https://doi.org/10.1088/0953-8984/24/21/216003 (2012).
15. Samudrala, G. K., Tsoi, G. M., Weir, S. T. & Vohra, Y. K. Structural and magnetic phase transitions in gadolinium under high pressures and low temperatures. *High Press. Res.* **34**, 385–391. https://doi.org/10.1080/08957959.2014.977277 (2014).
16. Thomas, S. A. *et al.* Neutron diffraction and electrical transport studies on magnetic ordering in terbium at high pressures and low temperatures. *High Press. Res.* **33**, 555–562. https://doi.org/10.1080/08957959.2013.806503 (2013).
17. Samudrala, G. K., Tsoi, G. M., Weir, S. T. & Vohra, Y. K. Magnetic ordering temperatures in rare earth metal dysprosium under ultrahigh pressures. *High Press. Res.* **34**, 266–272. https://doi.org/10.1080/08957959.2014.903946 (2014).
18. Lim, J., Fabbris, G., Haskel, D. & Schilling, J. S. Magnetic ordering at anomalously high temperatures in Dy at extreme pressures. *Phys. Rev. B* **91**, 045116. https://doi.org/10.1103/PhysRevB.91.045116 (2015).
19. Lim, J., Fabbris, G., Haskel, D. & Schilling, J. S. Anomalous pressure dependence of magnetic ordering temperature in Tb revealed by resistivity measurements to 141 GPa: Comparison with Gd and Dy. *Phys. Rev. B* **91**, 174428. https://doi.org/10.1103/PhysRevB.91.174428 (2015).
20. Lim, J., Fabbris, G., Haskel, D. & Schilling, J. S. Record high magnetic ordering temperature in a lanthanide at extreme pressure. *J. Phys. Conf. Ser.* **950**, 042025. https://doi.org/10.1088/1742-6596/950/4/042025 (2017).
21. Umebayashi, H., Shirane, G., Frazer, B. & Daniels, W. Neutron diffraction study of Tb and Ho under high pressure. *Phys. Rev.* **165**, 688. https://doi.org/10.1103/PhysRev.165.688 (1968).
22. Kawano, S., Achiwah, N., Onodera, A. & Nakaid, Y. Neutron diffraction studies of pressure effects on magnetic structures of Tb. *Phys. B Condens. Matter* **180–181**, 46–48. https://doi.org/10.1016/0921-4526(92)90655-C (1992).
23. Perreault, C., Vohra, Y., dos Santos, A., Molaison, J. & Boehler, R. Magnetic ordering in rare earth metal dysprosium revealed by neutron diffraction studies in a large-volume diamond anvil cell. *High Press. Res.* **39**, 588–597. https://doi.org/10.1080/08957959.2019.1688800 (2019).
24. Perreault, C. S., Vohra, Y. K., dos Santos, A. M. & Molaison, J. J. Magnetic structure of antiferromagnetic high-pressure phases of dysprosium. *J. Magn. Magn. Mater.* **545**, 168749. https://doi.org/10.1016/j.jmmm.2021.168749 (2022).
25. Perreault, C., Vohra, Y., dos Santos, A. & Molaison, J. Neutron diffraction study of magnetic ordering in high pressure phases of rare earth metal holmium. *J. Magn. Magn. Mater.* **507**, 166843. https://doi.org/10.1016/j.jmmm.2020.166843 (2020).
26. Cunningham, N. C., Qiu, W. & Vohra, Y. K. Observation of complete regular trivalent rare earth sequence in heavy lanthanide metal holmium under high pressure. *High Press. Res.* **26**, 43–50. https://doi.org/10.1080/08957950600646097 (2006).
27. Bi, W. *et al.* Studies of magnetism in dysprosium under extreme pressures. In *APS March Meeting Abstracts*, Vol. 2017 of APS Meeting Abstracts, B35.015 (2017).
28. Koehler, W. C., Cable, J. W., Wilkinson, M. K. & Wollan, E. O. Magnetic structures of holmium. I. The virgin state. *Phys. Rev.* **151**, 414–424. https://doi.org/10.1103/physrev.151.414 (1966).
29. Pechan, M. J. & Stassis, C. Magnetic structure of holmium. *J. Appl. Phys.* **55**, 1900–1902. https://doi.org/10.1063/1.333513 (1984).
30. Simpson, J. A., McMorrow, D. F., Cowley, R. A. & Jehan, D. A. Trigonal interactions in holmium. *Phys. Rev. B* **51**, 16073–16082. https://doi.org/10.1103/PhysRevB.51.16073 (1995).
31. Achiwa, N., Kawano, S., Onodera, A. & Nakai, Y. Effects of pressure on the helical turn angle of holmium. *Le J. Phys. Colloq.* **49**, C8-349–C8-350. https://doi.org/10.1051/jphyscol:19888156 (1988).
32. Samudrala, G. K. & Vohra, Y. K. Chapter 257–Structural properties of lanthanides at ultra high pressure. In *Including Actinides, Vol. 43 of Handbook on the Physics and Chemistry of Rare Earths* (eds Bünzli, J.-C.G. & Pecharsky, V. K.) 275–319 (Elsevier, 2013). https://doi.org/10.1016/B978-0-444-59536-2.00004-0.
33. Janner, A. & Janssen, T. Symmetry of incommensurate crystal phases. I. Commensurate basic structures. *Acta Crystallogr. Sect. A* **36**, 399–408. https://doi.org/10.1107/s0567739480000885 (1980).
34. Perez-Mato, J. M., Ribeiro, J. L., Petricek, V. & Aroyo, M. I. Magnetic superspace groups and symmetry constraints in incommensurate magnetic phases. *J. Phys. Condens. Matter* **24**, 163201. https://doi.org/10.1088/0953-8984/24/16/163201 (2012).
35. Rodríguez-Carvajal, J. & Villain, J. Magnetic structures. *C. R. Phys.* **20**, 770–802. https://doi.org/10.1016/j.crhy.2019.07.004 (2019).
36. Besson, J. *et al.* Neutron powder diffraction above 10 GPa. *Phys. B Condens. Matter* **180–181**, 907–910. https://doi.org/10.1016/0921-4526(92)90505-M (1992).

37. Klotz, S., Strässle, T., Rousse, G., Hamel, G. & Pomjakushin, V. Angle-dispersive neutron diffraction under high pressure to 10 GPa. *Appl. Phys. Lett.* **86**, 031917. https://doi.org/10.1063/1.1855419 (2005).
38. Klotz, S. *et al.* Advances in the use of Paris-Edinburgh presses for high pressure neutron scattering. *J. Neutron Res.* **21**, 117–124. https://doi.org/10.3233/jnr-190120 (2020).
39. Otto, J. W., Vassiliou, J. K. & Frommeyer, G. Nonhydrostatic compression of elastically anisotropic polycrystals. I. Hydrostatic limits of 4:1 methanol-ethanol and paraffin oil. *Phys. Rev. B* **57**, 3253. https://doi.org/10.1103/PhysRevB.57.3253 (1998).
40. Rodríguez-Carvajal, J. Recent advances in magnetic structure determination by neutron powder diffraction. *Phys. B Condens. Matter* **192**, 55–69. https://doi.org/10.1016/0921-4526(93)90108-I (1993).
41. Stokes, H. T., Hatch, D. M. & Campbell, B. J. ISODISTORT, ISOTROPY software suite. iso.byu.edu (2017).
42. Campbell, B. J., Stokes, H. T., Tanner, D. E. & Hatch, D. M. ISODISPLACE: A web-based tool for exploring structural distortions. *J. Appl. Crystallogr.* **39**, 607–614. https://doi.org/10.1107/s0021889806014075 (2006).
43. Aroyo, M. I. *et al.* Crystallography online: Bilbao crystallographic server. *Bulg. Chem. Commun.* **43**, 183–197 (2011).
44. Aroyo, M. I. *et al.* Bilbao crystallographic server: I. Databases and crystallographic computing programs. *Z. Krist. Cryst. Mater.*https://doi.org/10.1524/zkri.2006.221.1.15 *(2006).*
45. Aroyo, M. I., Kirov, A., Capillas, C., Perez-Mato, J. M. & Wondratschek, H. Bilbao crystallographic server. II. Representations of crystallographic point groups and space groups. *Acta Crystallogr. Sect. A Found. Crystallogr.* **62**, 115–128. https://doi.org/10.1107/s0108767305040286 (2006).
46. Perez-Mato, J. *et al.* Symmetry-based computational tools for magnetic crystallography. *Annu. Rev. Mater. Res.* **45**, 217–248. https://doi.org/10.1146/annurev-matsci-070214-021008 (2015).
47. Klotz, S., Chervin, J.-C., Munsch, P. & Marchand, G. L. Hydrostatic limits of 11 pressure transmitting media. *J. Phys. D Appl. Phys.* **42**, 075413. https://doi.org/10.1088/0022-3727/42/7/075413 (2009).
48. Bouad, N., Chapon, L., Marin-Ayral, R.-M., Bouree-Vigneron, F. & Tedenac, J.-C. Neutron powder diffraction study of strain and crystallite size in mechanically alloyed PbTe. *J. Solid State Chem.* **173**, 189–195. https://doi.org/10.1016/S0022-4596(03)00017-3 (2003).
49. Mao, H. *et al.* High-pressure phase transition and equation of state of lead to 238 GPa. *Solid State Commun.* **74**, 1027–1029. https://doi.org/10.1016/0038-1098(90)90479-U (1990).
50. Vohra, Y. K. & Ruoff, A. L. Static compression of metals Mo, Pb, and Pt to 272 GPa: Comparison with shock data. *Phys. Rev. B* **42**, 8651–8654. https://doi.org/10.1103/PhysRevB.42.8651 (1990).
51. Bak, P. & Mukamel, D. Physical realizations of n ≥ 4-component vector models. III. Phase transitions in Cr, Eu, MnS_2, Ho, Dy, and Tb. *Phys. Rev. B* **13**, 5086–5094. https://doi.org/10.1103/physrevb.13.5086 (1976).
52. Eckert, J. & Shirane, G. A neutron diffraction determination of the critical exponent β for the n = 4 system holmium. *Solid State Commun.* **19**, 911–912. https://doi.org/10.1016/0038-1098(76)90684-0 (1976).
53. Thurston, T. R. *et al.* Observation of two length scales in the magnetic critical fluctuations of holmium. *Phys. Rev. Lett.* **70**, 3151–3154. https://doi.org/10.1103/physrevlett.70.3151 (1993).
54. Thurston, T. R. *et al.* X-ray- and neutron-scattering measurements of two length scales in the magnetic critical fluctuations of holmium. *Phys. Rev. B* **49**, 15730–15744. https://doi.org/10.1103/physrevb.49.15730 (1994).
55. Plakhty, V. P. *et al.* Chiral criticality in helimagnet Ho studied by polarized neutron scattering. *Phys. Rev. B*https://doi.org/10.1103/physrevb.64.100402 *(2001).*

Acknowledgements

Author contributions

The authors contributed to the work as a team.

Competing interests

The authors declare no competing interests.

Additional information

Correspondence and requests for materials should be addressed to J.C.

Reprints and permissions information is available at www.nature.com/reprints.

Publisher's note Springer Nature remains neutral with regard to jurisdictional claims in published maps and institutional affiliations.